

## **Supporting Information**

### **Quinolinediol molecule electrode and MXene for asymmetric supercapacitor with efficient energy storage**

Long Jiao, Fuquan Ma, Xiaotong Wang, Zhimin Li, Zhongai Hu\*, Qing Yin

Key Laboratory of Eco-Environment-Related Polymer Materials of Ministry of Education, Key Laboratory of Polymer Materials of Gansu Province, College of Chemistry and Chemical Engineering, Northwest Normal University, Lanzhou, Gansu 730070, China.

\* Corresponding author – Email: zhongai@nwnu.edu.cn

#### **Material Characterizations**

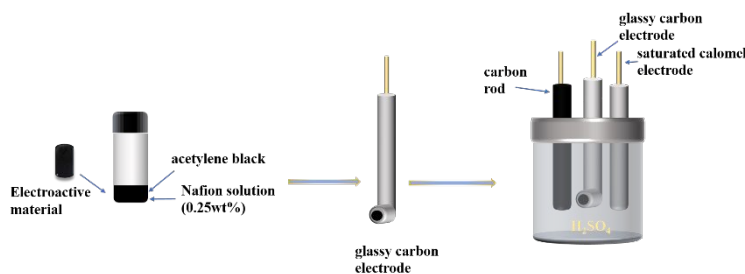
The morphology of the samples was observed by using scanning electron microscope (SEM, Ultra Plus, Carl Zeiss, Germany) and transmission electron microscope (TEM, JEM-2100 (Japan)). FTIR spectroscopy was analyzed through a Nicolet Nexus 670 instrument. The Raman spectra analysis was researched with an InVia Raman spectrometer (Renishaw) using a 514 nm argon ion laser. X-ray diffraction (XRD) analysis was generated using a diffractometer (D/Max-2400) with Cu K $\alpha$  radiation ( $\lambda = 1.5418 \text{ \AA}$ ) at 40 kV, 100 mA. Thermogravimetric (TG) analysis was accomplished on a PerkinElmer TG/DTA-6300 instrument from 20 to 800 °C at a heating rate of 5 °C min $^{-1}$  in N<sub>2</sub> atmosphere. Surface elemental analysis was carried out with X-ray photoelectron spectroscopy (XPS) via monochromatic Al K $\alpha$  radiation source (ThermoVG Scientific).

#### **Electrochemical performance test**

Cyclic voltammetry (CV), galvanostatic charge/discharge (GCD) and electrochemical impedance spectroscopy (EIS) were performed on a CHI760e electrochemical workstation (Chenghua, Shanghai, China) at room temperature. LANHECT2001A testing system (Wuhan LAND electronics Co., Ltd) is used for cycling stability test.

### The fabrication and electrochemical measurement of working electrodes

The fabrication of working electrodes: electrode materials (4 mg) and acetylene black (0.7mg) were uniformly dispersed in Nafion solution (0.25wt%, 0.4 mL). The above dispersion (6  $\mu$ L) was dripped onto the glassy carbon electrode by pipet gun. The electrochemical performances of electrode materials are tested in three electrode cell, which employs the glassy carbon electrode as the fluid collector, saturated calomel electrode (SCE) as the reference electrode, carbon rod as the counter electrode and 1 M  $H_2SO_4$  solution as electrolyte (Scheme S1).



**Scheme S1.** The preparation process of electrode.

### Calculations of capacitive characteristics

The specific capacitance ( $C$ ,  $F g^{-1}$ ) of active materials or asymmetric supercapacitor from the CV curves was calculated, according to the following equation:

$$C = \frac{\int IdV}{mv\Delta V} \quad (S1)$$

where  $I$ ,  $\Delta V$ ,  $v$  and  $m$  are the discharging current, the potential window, the potential scan rate and the mass of active material, respectively.

To construct the asymmetric supercapacitors, the masses of the positive and negative electrodes were balanced using the following formula:

$$\frac{m_+}{m_-} = \frac{C_- \times \Delta V_-}{C_+ \times \Delta V_+} \quad (\text{S2})$$

Where  $m$ ,  $C$ ,  $\Delta V$  with positive and negative signs are the mass, capacitance of single electrodes, and applied potential range of the positive and negative electrodes, respectively.

The energy density ( $\text{Wh kg}^{-1}$ ) and power density ( $\text{kW kg}^{-1}$ ) of the ASC device can be calculated according to equations:

$$E = \frac{\int I V(t) dt}{m} \quad (\text{S3})$$

$$P = \frac{E}{t} \quad (\text{S4})$$

where  $I$  is the discharging current,  $t$  is discharging time,  $V(t)dt$  is the integral area of the discharge curve and  $m$  is the mass of the active material.

### Positive materials characterization

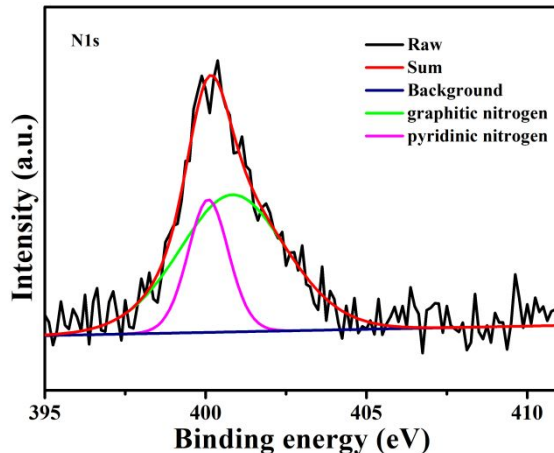


**Figure S1.** High-resolution N1s spectrum of QD/rGO-0.75

### Electrochemical measurements of OMEs

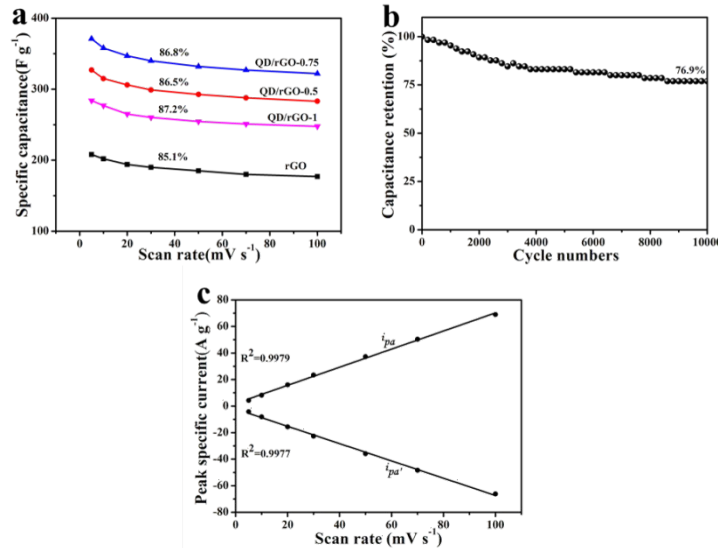


**Figure S2.** (a) Specific capacitance of all samples at 5–100 mV s<sup>-1</sup>. (b) Cycling stability of QD/rGO-0.75. (c) Relationship of peak current and scan rate

**Table S1.** The Rct and Rs values of the samples

Sample	Rct	Rs
rGO	0.34	1.99
QD/rGO-0.5	0.40	1.89
QD/rGO-0.75	0.45	1.80
QD/rGO-1	0.51	1.87

### Negative materials characterizations

The microstructure of  $Ti_3C_2T_x$  is studied by SEM (Figure S3a). The sample shows two dimensional sheet structure. Figure S3b shows the TEM image of  $Ti_3C_2T_x$  shows thin and transparent sheets.<sup>[1]</sup> Figure S3c shows the XRD pattern of  $Ti_3C_2T_x$ . A sharp peak at  $6.3^\circ$  and weak peaks could be observed at  $13.3^\circ$ ,  $19.1^\circ$ ,  $26.5^\circ$ ,  $40.6^\circ$  and  $60.9^\circ$

corresponding to the (002), (004), (006), (008), (0012) and (110) planes, suggesting that  $\text{Ti}_3\text{C}_2\text{T}_x$  is successfully synthesized.<sup>[2]</sup> Moreover, the XPS spectrum for  $\text{Ti}_3\text{C}_2\text{T}_x$  shows Ti2p, C1s, N1s, O1s and F1s peaks (Figure S3d). The high-resolution Ti2p spectrum of  $\text{Ti}_3\text{C}_2\text{T}_x$  shows three doublets (Ti2p<sub>3/2</sub>-Ti2p<sub>1/2</sub>) (Figure S3e). The high-resolution C1s spectrum shows five binding energies of 281.7, 282.5, 284.8, 286.2, and 288.3 eV, corresponding to C-Ti, C-Ti-O, C-C, C-O, and O-C=O (Figure S3f). The XPS results are consistent with other reports,<sup>[3,4]</sup> further indicating that  $\text{Ti}_3\text{C}_2\text{T}_x$  is successfully synthesized.

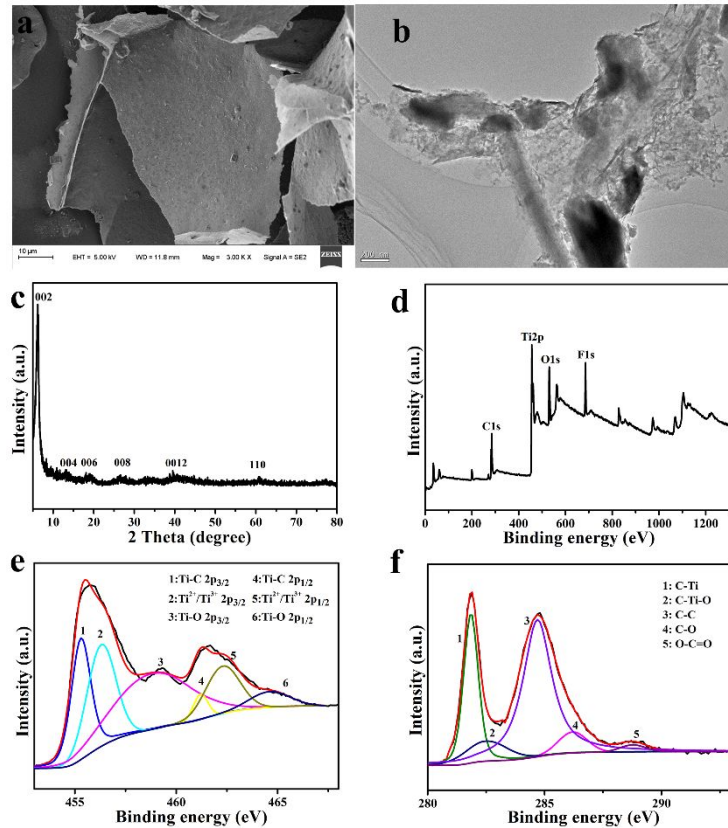


**Figure S3.** (a) SEM of  $\text{Ti}_3\text{C}_2\text{T}_x$ . (b) TEM of  $\text{Ti}_3\text{C}_2\text{T}_x$ . (c) XRD of  $\text{Ti}_3\text{C}_2\text{T}_x$ . (d) XPS spectra of  $\text{Ti}_3\text{C}_2\text{T}_x$ . (e) High-resolution Ti2p spectrum. (f) High-resolution C1s spectrum.

## Electrochemical measurements of $\text{Ti}_3\text{C}_2\text{T}_x$

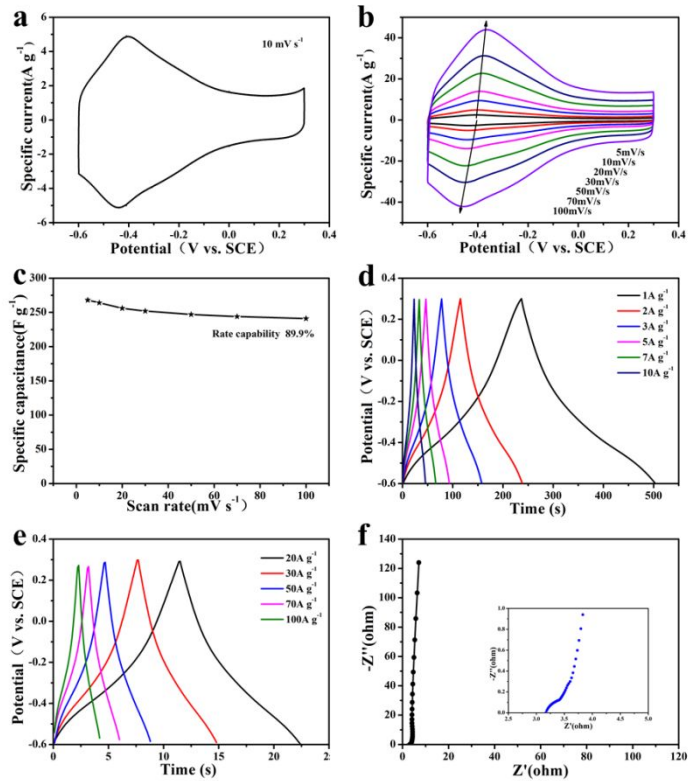


**Figure S4.** (a) CV curves of  $\text{Ti}_3\text{C}_2\text{T}_x$  at  $10 \text{ mV s}^{-1}$ . (b) CV curves of  $\text{Ti}_3\text{C}_2\text{T}_x$  at scan rate of  $5\text{--}100 \text{ mV s}^{-1}$  (c) Specific capacitance of  $\text{Ti}_3\text{C}_2\text{T}_x$  at scan rate of  $5\text{--}100 \text{ mV s}^{-1}$ . (d, e) GCD curves of  $\text{Ti}_3\text{C}_2\text{T}_x$  at  $1\text{--}100 \text{ A g}^{-1}$ . (f) Nyquist plots of  $\text{Ti}_3\text{C}_2\text{T}_x$  (The inset in (f) shows the magnified high-frequency region).

## Electrochemical measurement of ASC

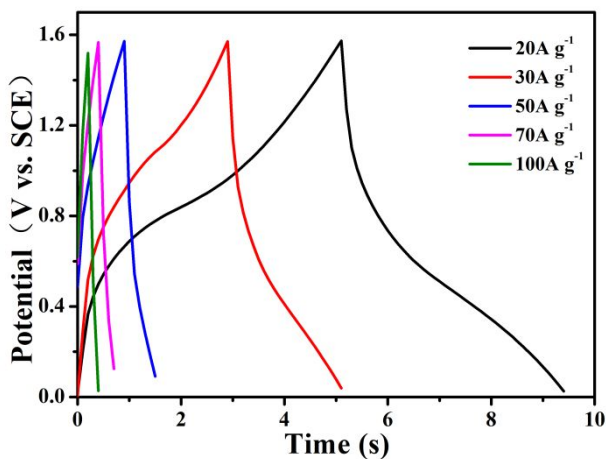


**Figure S5.** GCD curves of ASC at 20–100 A g<sup>-1</sup>.

## References

- [1] Tian, Y.; Yang, C.; Luo, Y.; Zhao, H.; Du, Y.; Kong, L. B.; Que, W. Understanding MXene-based “symmetric” supercapacitors and redox electrolyte energy storage. *ACS Appl. Energy Mater.* **2020**, *3*, 5006-5014.
- [2] Alhabeb, M.; Maleski, K.; Anasori, B.; Lelyukh, P.; Clark, L.; Sin, S.; Gogotsi, Y. Guidelines for synthesis and processing of two-dimensional titanium carbide ( $Ti_3C_2T_x$  MXene). *Chem. Mater.* **2017**, *29*, 7633-7644.
- [3] Shang, T.; Lin, Z.; Qi, C.; Liu, X.; Li, P.; Tao, Y.; Yang, Q. H. 3D macroscopic architectures from self - assembled MXene hydrogels. *Adv. Funct. Mater.* **2019**, *29*, 1903960.
- [4] Yan, J.; Ren, C. E.; Maleski, K.; Hatter, C. B.; Anasori, B.; Urbankowski, P.; Gogotsi, Y. Flexible MXene/graphene films for ultrafast supercapacitors with

outstanding volumetric capacitance. *Adv. Funct. Mater.* **2017**, *27*, 1701264.